ELSEVIER

Computer Physics Communications 146 (2002) 166–187

Computer Physics Communications

www.elsevier.com/locate/cpc

Numerical modeling of the coupling of an ICRH antenna with a plasma with self-consistent antenna currents

S. Pécoul [a], S. Heuraux [a,*], R. Koch [b], G. Leclert [c]

[a] *LPMI, Unité CNRS 7040, Université Henri Poincaré Nancy, 54506 Vandœuvre Cedex, France*
[b] *Lab. Physique des Plasmas, Lab. Plasmafysica, Association "Euratom-Etat Belge", Associate "Euratom-Belgische Staat", Ecole Royale Militaire, Koninklijke Militaire School, B1040 Brussels, Belgium*
[c] *LPIIM, Equipe Turbulence Plasma, Unité CNRS 6633, Université de Provence, Centre de St Jérôme, Case 321, 13397 Marseille Cedex 20, France*

Received 23 July 2001; received in revised form 3 December 2001; accepted 19 January 2002

Abstract

A realistic modeling of ICRH antennas requires the knowledge of the antenna currents. The code ICANT determines self-consistently these currents and, as a byproduct, the electrical characteristics of the antenna (radiated power, propagation constants on straps, frequency response,...). The formalism allows for the description of three-dimensional antenna elements (for instance, finite size thick screen blades). The results obtained for various cases where analytical results are available are discussed. The resonances appearing in the spectrum and the occurrence of unphysical resonant modes are discussed. The capability of this self-consistent method is illustrated by a number of examples, e.g., fully conducting thin or thick screen bars leading to magnetic shielding effects, frequency response and resonances of an end-tuned antenna, field distributions in front of a Tore-Supra type antenna with tilted screen blades.

PACS: 52.40.Fd; 52.50.Qt

Keywords: Self-consistent antenna currents; Three-dimensional antenna modeling; Finite Faraday screen; EM field near the antenna

1. Introduction

Many tokamaks use antennas launching a wave in the ion cyclotron range of frequencies (ICRF), with a high amount of power (typically up to more than 10 MW). It is therefore important to optimize the antenna design and its coupling to the plasma in order to reduce the voltages, electric fields and possibly the losses at the plasma edge. Since the measurements on actual antennas cannot easily be made in the presence of the plasma, one has to rely upon numerical simulations. One therefore wants codes as realistic as possible. Many papers have been devoted to this problem, starting more than twenty years ago [1]. The first coupling theory is based on the "induced-EMF"

* Corresponding author.
E-mail addresses: serge.pecoul@lpmi.uhp-nancy.fr (S. Pécoul), stephane.heuraux@lpmi.uhp-nancy.fr (S. Heuraux), r.koch@fz-juelich.de (R. Koch), leclert@up.univ-mrs.fr (G. Leclert).

0010-4655/02/$ – see front matter
PII: S0010-4655(02)00269-2

method [2,3]. Soon after, the variational method was proposed [4] and used in many subsequent works [5,6]. Further developments aimed at the description of a more complex geometry, like the work in [7], which allows considering antennas imbedded in nested boxes. These methods are basically not self-consistent because current density profiles are specified on each part of the antenna rather than being determined from the metallic boundary conditions at the surface of the conductors. Self-consistency is used in the ARGUS code to treat vacuum problems [8,9]. Recently a new analytical method has been used to evaluate the Green functions necessary to compute the current distribution on the IGNITOR antenna structure [10]. Some codes are based on finite (volume-) element method, but they need too much time to describe a realistic antenna facing an inhomogeneous plasma [11]. One can find more general information on this area in the review papers [12,13].

An efficient way of improving the possibility to deal with realistic antenna structures is to implement the self-consistency of the antenna currents in the formalism from the very beginning [14]. The purpose of the paper is to describe the implementation of this idea and the resulting code, ICANT, which calculates these self-consistent currents on every part of the antenna. Once the currents are known, any electrical property can be determined: the input impedance, the radiated power, the electromagnetic field ($\mathbf{E}, \mathbf{B}$) in the whole region between the torus wall and the plasma and so on. The plasma interface is described by the usual surface impedance matrix whose sophistication depends upon the number of modes allowed to propagate into the plasma (fast, slow, Bernstein, ...). In this article, we focus on the computational aspects of the method, and shall give examples for the most simple case of the surface impedance matrix for the fast wave propagation only.

The paper is organized as follows. Section 2 sets up the basic equations and assumptions of the model. In Section 3 the impedance matrix for simple plasma wave models involving only the fast wave is given. In Section 4, the computational aspects of the work are presented in greater details. Section 5 deals with simple cases in order to compare the numerical results with the analytical results obtained from the transmission line theory. These results are shown to be in excellent agreement. This is the occasion to discuss the physical interpretation of resonances of the propagation constant which appear in the solution. In Section 6, we show that allowing the currents to flow in any direction on the antenna leads to the existence of magnetic shielding effects; their influence on the radiated power is discussed to some extent. In Section 7, the features of the solution in the presence of plasma are described in several examples as the self-consistent current distribution of a tunable strap antenna or the modeling of thick Faraday screens. Finally, an interesting feature of the code is exhibited: the field can be computed over the whole vacuum region, in particular between the screen (or the strap itself in the absence of Faraday screen) and the plasma edge. Results are presented and discussed for a Tore-Supra-like antenna.

2. The basic assumptions and the self-consistency condition

Although we aim at modeling possibly complicated structures, we need a few assumptions that can more or less reduce the mathematical complexity of the model.

2.1. The plasma slab approximation

The coupling problem focuses on the behaviour of the fields in the vicinity of the antenna, hence the radial distances over which we want to solve the problem are short compared with both the poloidal extent of the antenna and the plasma radius. It is then customary to work with a Cartesian frame (Fig. 1) where the radial direction is along the x-axis, and the poloidal and toroidal directions are along the y- and z-axis. The plasma is assumed homogeneous in the y- and z-directions, and inhomogeneous in the x-direction. The periodicities of the toroidal geometry are kept by imposing a periodicity length $L_y = 2\pi a$ in the y-direction and $L_z = 2\pi R$ in the z-direction, where a and R are the minor and major radius. It results that the problem can be Fourier analyzed in the poloidal and toroidal directions, and the inverse Fourier transforms are series of the form

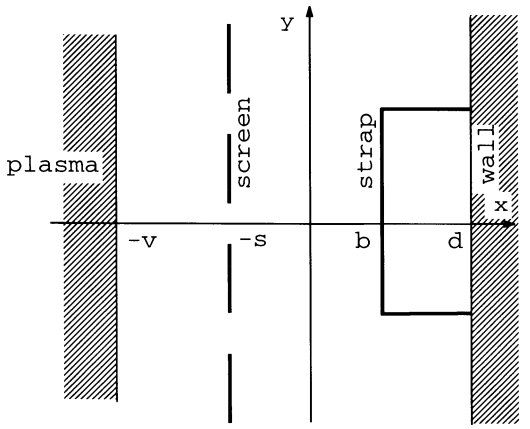

Fig. 1. The slab geometry for the antenna-plasma system. The z-coordinate is perpendicular to the figure plane. $-v$, $-s$, b and d are the positions of the plasma-vacuum interface, the screen, the strap and the wall for the simplest case.

$$f(x,y,z)=\frac{1}{4\pi^2 aR}\sum_{n=-\infty}^{n=\infty}\sum_{m=-\infty}^{m=\infty} f(x,m/a,n/R)\exp\bigl[\mathrm{i}(my/a+nz/R)\bigr]. \tag{1}$$

The notation $k_y = m/a$ and $k_z = n/R$ will often be used in the following.

2.2. The vacuum-plasma interface

One major underlying assumption is that there is always some vacuum layer between the wall and the plasma edge. This allows us to solve the problem between two planes, the torus wall at $x = d$, and some plane at $x = -v$ where we impose a boundary condition describing the plasma properties behind this plane. This boundary condition only requires the knowledge of the surface impedance of the plasma, which means that any plasma model, based on Fourier transformation in y and z, can be coupled to the ICANT code. In practice, in addition to the simple models of pure vacuum or uniform plasma, one often adopts a description where the fast wave only is propagating; cold or warm descriptions of this wave can be adopted [15] without significant increase of the complexity. Likewise, one can equally easily use a reflection boundary condition at the inboard side of the plasma or use a radiation condition at some location in the plasma to mimic complete absorption by the plasma. The latter model, usually called "single pass absorption" model, is the most frequently used, in particular for engineering purposes, because it describes only the antenna-plasma coupling properties. Additional complexity can come from cavity modes that may build up inside the plasma and that lead to large variations in the antenna properties when plasma parameters are varied.

2.3. The formal solution for the field

We recall here the expressions of the electromagnetic field in terms of the currents [14]. In the plasma slab approximation, the Fourier components of the transverse fields (E_x, E_y), (B_x, B_y) can be expressed in terms of the longitudinal fields E_z and B_z and the local current density $\mathbf{J}$

$$\begin{aligned}
\begin{pmatrix} B_x \\ E_y \end{pmatrix} &= \frac{1}{H^2}\begin{bmatrix} -\mathrm{i}\omega/c^2 & \mathrm{i}k_z \\ \mathrm{i}k_z & -\mathrm{i}\omega \end{bmatrix}\begin{pmatrix} \mathrm{i}k_y E_z \\ \mathrm{d}B_z/\mathrm{d}x + \mu_0 J_y \end{pmatrix}, \\
\begin{pmatrix} E_x \\ B_y \end{pmatrix} &= \frac{1}{H^2}\begin{bmatrix} -\mathrm{i}\omega & \mathrm{i}k_z \\ -\mathrm{i}k_z & \mathrm{i}\omega/c^2 \end{bmatrix}\begin{pmatrix} -\mathrm{i}k_y B_z + \mu_0 J_x \\ \mathrm{d}E_z/\mathrm{d}x \end{pmatrix}.
\end{aligned} \tag{2}$$

c is the velocity of light, μ_0 the permeability of free space and ω the wave frequency. The longitudinal Fourier components of the field obey the equation

$$\frac{\mathrm{d}^2\boldsymbol{\Psi}}{\mathrm{d}x^2} - p^2\boldsymbol{\Psi} = \boldsymbol{\Phi} \tag{3}$$

where $\boldsymbol{\Psi}$ and $\boldsymbol{\Phi}$ have the following meaning

$$\boldsymbol{\Psi} = \begin{pmatrix} cB_z \\ E_z \end{pmatrix}, \qquad \Phi = \begin{pmatrix} -\mu_0 c(\mathrm{d}J_y/\mathrm{d}x - \mathrm{i}k_y J_x) \\ [k_z(\mathrm{d}J_x/\mathrm{d}x + \mathrm{i}k_y J_y) - \mathrm{i}H^2 J_z]/(\varepsilon_0\omega) \end{pmatrix}. \tag{4}$$

In the previous equations, H and p stand for

$$H^2 = k_0^2 - k_z^2, \qquad p^2 = k_y^2 + k_z^2 - k_0^2, \tag{5}$$

where $k_0 = \omega/c$ is the vacuum wavenumber. Once the Green's function of Eq. (3) is computed, the fields can be computed in terms of the currents from Eqs. (3) and (2). For instance, the electric field is

$$\mathbf{E}(x, k_y, k_z) = -\mathrm{i}\mu_0\omega \int_{-v}^{d} \mathbf{R}(x, \rho)\cdot\mathbf{J}(\rho)\,\mathrm{d}\rho - \mathrm{i}\mu_0 \frac{\omega}{k_0^2}\begin{pmatrix} J_x \\ 0 \\ 0 \end{pmatrix}. \tag{6}$$

R is deduced from the surface impedance matrix and its expression can be found in [14]. The spectral power is then obtained as

$$S(k_y, k_z) = \int_{-v}^{d} \mathrm{d}x\,\mathbf{E}\cdot\mathbf{J}^* = -\mathrm{i}\mu_0\omega \int_{-v}^{d}\int_{-v}^{d} \mathrm{d}x\,\mathrm{d}\rho\,\mathbf{J}^*(x)\cdot\mathbf{R}(x,\rho)\cdot\mathbf{J}(\rho) - \mathrm{i}\mu_0\omega k_0^{-2}\int_{-v}^{d} \mathrm{d}x\,J_x^*(x)J_x(x). \tag{7}$$

2.4. The boundary conditions

The torus wall is assumed metallic, so the tangential electric field is zero on this wall

$$E_z|_{x=d} = E_y|_{x=d} = 0. \tag{8}$$

At the vacuum-plasma interface, the most general boundary condition constitutes a set of two equations relating the longitudinal fields and their derivatives

$$\frac{\mathrm{d}\boldsymbol{\Psi}}{\mathrm{d}x} = \mathbf{b}\cdot\boldsymbol{\Psi} \quad \text{at } x = -v. \tag{9}$$

The coefficients of the matrix **b** can be deduced from the wave equation in the medium on the left ($x < -v$) of the boundary plane. The matrix **b** can be easily related to the surface impedance matrix ξ relating the electric and magnetic fields at the boundary plane $x = -v$

$$\begin{pmatrix} E_y \\ E_z \end{pmatrix}_{x=-v} = \xi \begin{pmatrix} \omega B_z \\ \omega B_y \end{pmatrix}_{x=-v}. \tag{10}$$

The general expression of ξ in terms of **b** is

$$\xi = \frac{1}{\mathrm{i}k_0^2 b_{22} H^2}\begin{bmatrix} k_0^2 b_{11}b_{22} - (k_0 b_{12} - \mathrm{i}k_y k_z)(k_0 b_{21} + \mathrm{i}k_y k_z) & -H^2(k_y k_z + \mathrm{i}k_0 b_{21}) \\ H^2(k_y k_z - \mathrm{i}k_0 b_{21}) & H^4 \end{bmatrix}. \tag{11}$$

For example, for an antenna in vacuum, the matrix **b** of the boundary condition reads

$$\mathbf{b} = \begin{pmatrix} -p & 0 \\ 0 & -p \end{pmatrix}. \tag{12}$$

If we want to model the polarizing role of the Faraday screen (FS), we set a boundary condition that forces the electric field component in the direction of the screen bars, say E_z, to vanish and $\mathbf{b}$ takes the form

$$\mathbf{b} = \begin{pmatrix} -p & 0 \\ 0 & +\infty \end{pmatrix}. \tag{13}$$

We call this case the ideal Faraday screen (IFS), in contrast with the finite Faraday screen (FFS), which will be modeled by finite blades carrying self-consistent currents.

3. The surface impedance matrix for the magnetosonic wave

As several examples hereafter will consider the excitation of the fast magnetosonic wave in the plasma, we discuss in this section the surface impedance matrix for this wave.

3.1. Homogeneous plasma

The dispersion relation is

$$k_\perp^2 = k_0^2 u\left(1-\mu^2\right), \quad u = \left(\epsilon_1 - k_z^2/k_0^2\right),\ \mu = \epsilon_2/u. \tag{14}$$

Here $k_\perp^2 \equiv k_x^2 + k_y^2$ and ϵ_1 and $\mathrm{i}\epsilon_2$ are components of the cold dielectric tensor

$$\epsilon = \begin{pmatrix} \epsilon_1 & \mathrm{i}\epsilon_2 & 0 \\ -\mathrm{i}\epsilon_2 & \epsilon_1 & 0 \\ 0 & 0 & \epsilon_3 \end{pmatrix},$$

$$\epsilon_1 = 1 - \sum_s \frac{\omega_{ps}^2}{\omega_2 - \omega_{cs}^2}, \quad \epsilon_2 = -\sum_s \frac{\omega_{cs}}{\omega}\frac{\omega_{ps}^2}{\omega^2 - \omega_{cs}^2}, \quad \epsilon_3 = 1 - \sum_s \frac{\omega_{ps}^2}{\omega^2} \tag{15}$$

with ω_{ps} and ω_{cs} the plasma and cyclotron frequencies of the plasma species s. The expression (14) is valid under the assumption that $|\epsilon_3| \gg |\epsilon_1|, |\epsilon_2|$. Under this condition, which is easily satisfied in the ion cyclotron frequency domain for not too low density, the fast and slow waves are uncoupled. Then for the fast wave [16] $E_z = 0$, so we can expect that the boundary condition will exhibit features similar to those of the IFS. Indeed, for the homogeneous plasma the surface impedance matrix is

$$\xi = \begin{bmatrix} \xi_{11} & 0 \\ 0 & 0 \end{bmatrix}, \quad \xi_{11} = -\mathrm{i}\left[\mu k_y - \mathrm{i}\left(k_\perp^2 - k_y^2\right)^{1/2}\right]/k_\perp^2 \tag{16}$$

and the matrix of the boundary conditions is

$$\mathbf{b} = \begin{bmatrix} b_{11} & 0 \\ 0 & +\infty \end{bmatrix}, \quad b_{11} = \mathrm{i}H^2\xi_{11}. \tag{17}$$

In fact, the IFS is the limit of the magnetosonic case for vanishing density.

3.2. Inhomogeneous plasma

The shape of the the edge density profile influences strongly the coupling efficiency [16]. The surface impedance matrix is then deduced from the solution of the coupled set of differential equations describing each Fourier component (k_y, k_z) of the fast wave:

$$\frac{\mathrm{d}}{\mathrm{d}x}\begin{bmatrix} \mathrm{i}\omega B_z \\ E_y \end{bmatrix} = \begin{bmatrix} -\mu k_y & -k_\perp^2 \\ 1 - k_y^2/(k_0^2 u) & \mu k_y \end{bmatrix}\begin{bmatrix} \mathrm{i}\omega B_z \\ E_y \end{bmatrix}. \tag{18}$$

This is done for instance by the BRAFFA code [15], which integrates the equations in a slab geometry. The output of this code is then used as an input for the boundary condition of the ICANT code. Finally, we note that the existence of other waves (slow mode, Bernstein waves) can be introduced in the impedance matrix, either analytically [17,18] or numerically.

4. The condition for current self-consistency and the code implementation

Since the antennas are considered as perfect conductors, the tangential electric field $\mathbf{E}_t$ must vanish at their surface (and similarly on screen blades, septas, etc.). This boundary condition will be implemented in a form that is consistent with the type of representation we shall adopt for the currents flowing at the surface of these perfect conductors.

4.1. Current element basis

We subdivide the surface of any conductor into a number of polygons (in practice, we use rectangles) delimiting a flat surface over which the current is flowing. Let us call S_i this elementary surface and call $\mathbf{e}_i$ any unitary vector lying inside the surface. Then we choose as current element the vector

$$\mathbf{T}_i = T_i(\mathbf{r})\mathbf{e}_i \Delta(S_i), \tag{19}$$

where $\Delta(S_i)$ is the characteristic function of S_i which, integrated in the direction of the normal to S_i yields 1 on the surface and 0 elsewhere. For example, a rectangular element located in a plane $x =$ constant will have as characteristic function

$$\Delta(S) = \delta(x - x_0)\gamma_{y_0}^{y_1}(y)\gamma_{z_0}^{z_1}(z),$$

where δ is the Dirac delta function and $\gamma_{y_0}^{y_1}(y)$ is the "door" function ($= 1$ for $y_0 < y < y_1$, $= 0$ else). $T_i(\mathbf{r})$ is an arbitrary function of the space co-ordinates, but will be chosen as linear in the following. $\mathbf{T}_i$ represents a unidirectional current, as if the surface S_i had anisotropic conductivity. To represent a current of arbitrary direction on the surface, two elements of the type (19) must be used. We thus decompose the unknown current flowing on the antenna parts on a basis of current elements $\mathbf{T}_j$

$$\mathbf{J} = \sum_{j=1}^{j=A} a_j \mathbf{T}_j + \sum_{j=1}^{j=N} c_j \mathbf{T}_j. \tag{20}$$

In this expression, the first sum represents the A *active* antenna elements, on which the currents (i.e. the a_j's) are known quantities. The second sum corresponds to the N *passive* antenna elements, where the currents are unknown. We thus have N coefficients c_j to determine and need N conditions. Although other choices could be made, a natural implementation of the condition of vanishing of the tangential electric field is to impose, for each unidirectional current element $\mathbf{T}_i$, the vanishing, in the average over the surface, of the electric field in the direction of conductivity:

$$\iint \int_{\text{vacuum}} \mathbf{E} \cdot \mathbf{T}_k^* \, \mathrm{d}V = 0, \quad k = 1, N \tag{21}$$

for each of the N current elements. The integral is over the vacuum region where the antenna is located. As a result the self-consistent determination of the currents reduces to the inversion of a set of linear equations

$$\sum_{j=1,N} c_j Q_{kj} = -\sum_{j=1,A} a_j Q_{kj}, \tag{22}$$

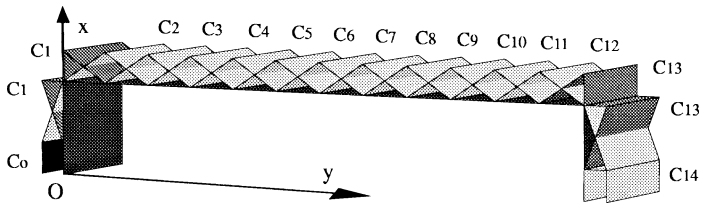

Fig. 2. Layout of the current elements for the single strap antenna with a one-dimensional current. The active element C_0 is the combination of a door function (in black) and a half-rooftop with equal amplitudes.

where the matrix **Q** is related to the matrix **R** by

$$Q_{kj} = -\mathrm{i}\omega\mu_0 \sum_{k_y,k_z} \iint \mathrm{d}x\,\mathrm{d}\rho\, \mathbf{T}_j \cdot \mathbf{R} \cdot \mathbf{T}_k^* - \frac{\mathrm{i}\omega\mu_0}{k_0^2} \sum_{k_y,k_z} \int \mathrm{d}x\, \mathbf{T}_{xj} \cdot \mathbf{T}_{xk}. \tag{23}$$

The solution of the problem involves two sums over the number of elements and two sums over the wave-numbers. The double integral on x and ρ can be performed analytically for a proper choice of the current basis; some care must be taken due to the discontinuity of the derivatives of the Green's function.

The above choice corresponds to the simplest form of the Galerkin method applied to the present boundary element representation. Note that this implementation allows naturally simplified models of the antenna (or other surrounding conductors) where the current only flows in a given direction (anisotropic conductivity), like in most simpler antenna models. The first applications we shall consider in the sequel will be of this kind. Such current distributions do not prevent the magnetic field from crossing conducting surfaces. Only the complete representation using bi-directional currents will prevent this, giving rise to what is called in the following "magnetic shielding" ($\mathbf{B} \cdot \mathbf{n}_i\, \Delta(S_i) = 0$, with $\mathbf{n}_i$ the normal to S_i).

There is much freedom in the choice of the current basis; as already mentioned a convenient basis can be made of current elements varying linearly by parts. In this case three elementary elements are used to model uni-directional antenna currents: the "door", the "rooftop" and the "half-rooftop". Due to the current continuity condition, the corners where the antenna surface changes direction must be treated with some care, since divergent terms arise from any departure to the continuity [14]. Special basis elements are designed to handle this problem. All current elements for a single strap antenna in the one-dimensional case are shown on Fig. 2. The active element (and similarly the element connecting the other end of the strap to the wall) is modeled by a combination of door and half-rooftop and the corner elements are pairs of half-rooftops with equal amplitudes. All other elements are overlapping rooftops. The size of the current elements is chosen as large as possible in accordance with the nature of the physical problem, in order to minimize the computation time. Of course this time is greatly increased if one assumes an isotropic conductivity (two-dimensional currents) on each part of the antenna structure.

Once the currents are determined, the fields and the power can be computed with the previous formulae. Their implementation in a Fortran code raises the questions of convergence and accuracy, which we now examine briefly.

4.2. Convergence tests

For the numerical calculation, Eq. (1) has to be truncated in the (k_y, k_z) space and only a finite number of modes (m, n) are taken. Hence calculated quantities reach their asymptotic value only if the limits of m and n are high enough. These limits depend on various parameters, such as the excited wavenumber k_0 and the minor and major radii a and R, but above all on the size of the smallest antenna element used in the antenna description. Good accuracy is generally obtained with a number of modes given by the inequalities $n > 3\pi R/\Delta w_z$ and $m > 3\pi a/\Delta w_y$ where Δw_z and Δw_y are the smallest dimensions of the antenna elements. However, lower limits (by a factor of 2 to 3) can be chosen if one wants only the current profile or the real part of the power, whereas the convergence is weaker for the imaginary part of the power. The calculation of the electromagnetic field near the

antenna needs generally more modes, because smaller antenna elements are required to accurately describe steep field gradients that can occur locally (roughly speaking the shortest gradient lengths that can be resolved are of the order of half the element size). For example, with the above criterion, for a single strap in vacuum (see Section 5), the electric field structure varies by less than 1% once more than 10 current elements are used to model the strap.

As we use a Galerkin method, it is expected that the condition that the tangential electric field vanishes on conductors is satisfied on the average, and the maximal residual value of the tangential electric field decreases with the number of elements. For instance, with a strap antenna and its finite Faraday screen, for 10 current elements on the strap and 7 current elements on each screen blade the maximal residual value of E_z on the strap, normalized to the value of E_z in the screen plane between the blades, is 2.5%. For 15 current elements on the strap it decreases to 1%.

On the other hand the maximal number of elements is bounded due to the memory size of the computer and the computation time. Note also that the computation time increases much more rapidly than the number of elements, because taking more elements means also taking more modes. A realistic example is the Tore-Supra Q1 antenna [28], with two straps and their Faraday shield. At a frequency of 48 MHz, with $a = 0.74$ m and $R = 2.35$ m, with 697 current elements (element size of 3 cm), the spatial resolution of the fields is of the order of 1 cm with 300 k_y-modes and 900 k_z-modes. Finally, for the calculation of the 16-strap ITER antenna, at a frequency of 55 MHz, with $a = 2$ m and $R = 6.2$ m and an element size of 6 cm (2400 current elements), a spatial resolution of 2 cm for the fields requires 600 k_y-modes and 2000 k_z-modes. The accuracy remains acceptable with 7 current elements on each strap, the error tangential electric field on the strap (normalized as above) being less than 5%. For this last case the main limit comes from the available memory size, 1 Go, and the computation time is 14 days on a DEC-Alpha workstation with a 666 MHz processor.

5. The antenna in vacuum

This section is devoted to very simple situations that allow the comparison of the code results with analytical predictions.

5.1. Single strap antenna in free-space

The simplest case which can be studied is the case of a single strap antenna radiating in vacuum. For simplicity, we consider here only one-directional currents. The strap has a length $2w_y$ and a width $2w_z$. The distance between the wall and the strap is $d - b$. The feeder (the *active* element) is the element parallel to x at $y = 0$, where we impose a unit current (1 A) and the current density of this active element in Eq. (20) is computed accordingly. We want to determine the unknown currents J_y on the strap, and J_x on the short-circuit (Fig. 2). For this case the propagation constant, as follows from the transmission line theory, is $\beta = k_0$. Moreover, an analytical expression of the radiated power [19] exists in the 2D limit, $J_x = 0$, $|b - d| \ll w_y$, w_z and $k_0 w_z \ll 1$. For a 1 A current at the feeder, the radiated power (in W) is

$$P_{\text{rad}} = \frac{1}{4\pi}\sqrt{\frac{\mu_0}{\varepsilon_0}}\,k_0^2(d-b)^2\left[1 - \frac{\sin(4k_0 w_y)}{4k_0 w_y}\right]. \tag{24}$$

Fig. 3 compares this expression with the numerical results obtained for large values of R and a, $R = a = 10$ m. The strap parameters are $d = v = 0.004$ m, $b = 0$, $w_y = 0.5$ m and $w_z = 0.125$ m (hereafter we will always take $b = 0$ in numerical calculations). One sees that there is a good agreement over a broad range of frequencies. However, a closer look at the results shows that the dispersion of the numerical points is not due to a lack of accuracy, but arises from the difference between radiation in free (infinite) space and radiation in a periodic medium, which is implicitly assumed in the present computations (§2.1). For this particularly simple case, where the boundary matrix

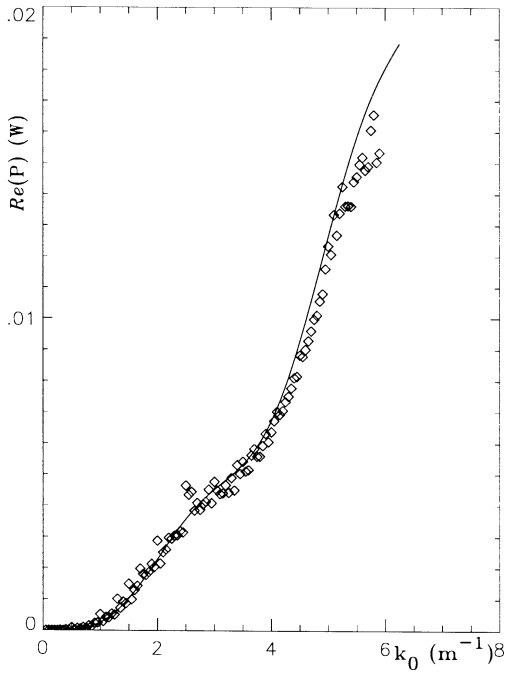

Fig. 3. The power radiated by a single strap antenna in vacuum. $R = 10$ m, $a = 10$ m, $d = v = 0.004$ m, $w_y = 0.5$ m and $w_z = 0.125$ m. The solid line corresponds to the 2D theory, Eq. (24).

b reduces to a diagonal, Eq. (12), the expression of the spectral power (7) can be recast into the simple form [20] (written for $b = 0$ without loss of generality):

$$\frac{S}{-\mathrm{i}\omega\mu_0} = \frac{1-\mathrm{e}^{-2pd}}{2pk_0^2}\left\{|J_x + \mathrm{i}k_y J_y|^2 - k_0^2|J_y|^2\right\} + \left(\frac{1-\mathrm{e}^{-2pd}}{2pd} - 1\right)\frac{d|J_x|^2}{p^2}. \tag{25}$$

This expression has a singularity at $p = 0$ which behaviour can be made more explicit by expanding the exponential $\exp(-2pd)$ to second order in its argument:

$$\frac{S}{-\mathrm{i}\omega\mu_0} = \frac{(1-pd)d}{k_0^2}\left\{|J_x + \mathrm{i}k_y J_y|^2 - k_0^2|J_y|^2\right\} - \frac{d^2}{p}|J_x|^2. \tag{26}$$

This expression has a simple pole at $p = (k_y^2 + k_z^2 - k_0^2)^{1/2} = 0$. In free space, when computing the total radiated power by inverse Fourier transform, this appears as an integrable singularity in the (k_y, k_z) spectrum. However, in the periodic geometry implicitly assumed here, there will be large (infinite) contributions to the active radiated power (which comes from the part of the spectrum $p^2 \leqslant 0$) when the poloidal and toroidal mode numbers nearly (exactly) satisfy the relation

$$k_0^2 = (n/R)^2 + (m/a)^2. \tag{27}$$

This relation is the cut-off condition for vacuum waves. The presence of the $1/p$ singularity in the expression of the radiated power is responsible for a fine structure which is not resolved in the curve of $P(k_0)$ in Fig. 3. A detail of such a curve is shown on Fig. 4, where the first resonance appears at $k_0 = 1/R$. Here $R = 4$ m, $a = 2$ m, and the other parameters are the same as previously. For lower frequencies, only the term at $(k_y, k_z) = (0, 0)$ contributes to the real part of the radiated power. The condition $p = 0$, Eq. (27), corresponds to the existence of eigenmodes of the periodic system. Variants of these are encountered in other situations, e.g., in the case of a high density plasma, or

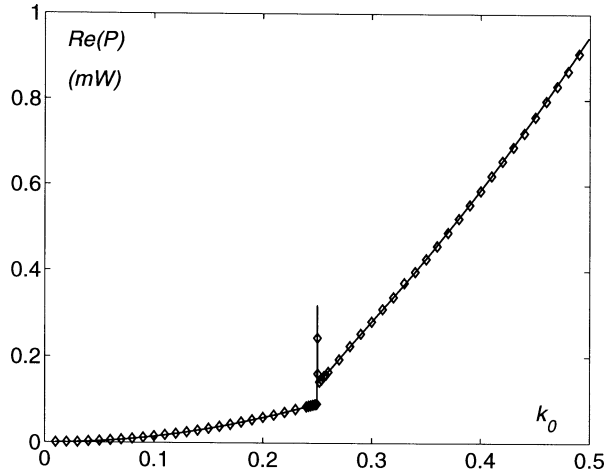

Fig. 4. First resonance of the radiated power $\mathrm{Re}(P)$ for the single strap antenna in vacuum. The parameters are the same as on Fig. 3, except $R = 4$ m and $a = 2$ m. $\diamond$: ICANT results. Solid line: analytical results from expression (25).

when the plasma is replaced by a metallic wall. In the latter cases, these modes have been called "coaxial", because they are similar to those propagating in a coaxial cavity (here the plasma plays the role of the central conductor). It is worth noticing that these modes are excited by radial currents ($J_x \neq 0$). The fine structure associated with these resonances has been investigated in more detail in [20].

5.2. The strap antenna with an ideal Faraday screen

The case of the strap antenna with an ideal Faraday screen in vacuum is interesting, because it is the way many codes model the screen, and also because, as mentioned, it is the low density limit of the magnetosonic surface impedance matrix. Since the IPS is modeled through the matrix of boundary conditions (13), $s = v$. In this case, the normalized propagation constant along the antenna is no longer 1. Its quasi-static limit (with the inductance and capacitance per unit length calculated at zero frequency, $k_0 \to 0$) is well-known in transmission line theory [21]

$$\beta = k_0 \left(\frac{d+s}{b+s} \right)^{1/2}, \tag{28}$$

where $x = b$ is the location of the central conductor. In the 2D (but not quasi-static) limit and under the same assumptions as for Eq. (24), one gets [21]

$$\begin{aligned} \beta^2 &= k_0^2 \frac{d+s}{b+s+(d-b)S}, \\ S &= \left\{ 1 - \frac{\sin(k_0 w_z)\sin[k_0 R(\pi - w_z/R)]}{k_0 w_z \sin(k_0 \pi R)} \right\}. \end{aligned} \tag{29}$$

One can see that β goes to infinity for values of k_0 slightly lower than n/R. More important, the phase velocity ω/β exhibits resonances at $k_0 = n/R$ (equivalently $H^2 = 0$). These resonances also appear in the expression of the radiated power:

$$\begin{aligned} \frac{S}{-\mathrm{i}\omega\mu_0} = \frac{1-\mathrm{e}^{-2pd}}{2p} &\left\{ \frac{1}{H^2} |J_x + \mathrm{i}k_y J_y|^2 - |J_y|^2 + \frac{1}{p^2} |J_x|^2 \right\} \\ &- \frac{d}{p^2} |J_x|^2 - \frac{k_z^2}{k_0^2 H^2} |J_x + \mathrm{i}k_y J_y|^2 \frac{\sinh ps \sinh pd}{p \sinh p(d+s)}. \end{aligned} \tag{30}$$

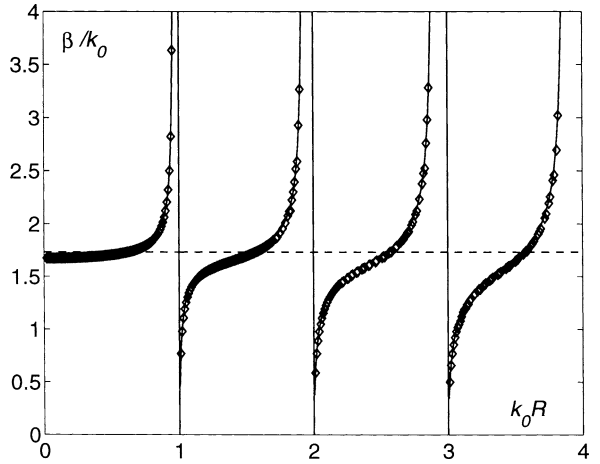

Fig. 5. Variation of the normalized propagation constant β/k_0 with the frequency tor the single strap antenna in vacuum with an ideal Faraday screen. $R = a = 2$ m, $d = 0.004$ m, $s = v = 0.002$ m, $w_y = 0.5$ m and $w_z = 0.125$ m. $\diamond$: ICANT results. The solid line is Eq. (29). The dotted line corresponds to the static limit, Eq. (28).

This expression has the same (integrable) singularity for $p \to 0$ as in the vacuum case, namely

$$\frac{S}{-\mathrm{i}\omega\mu_0} \to -\frac{d^2|J_x|^2}{p} \tag{31}$$

but in addition, it exhibits new resonances at $H^2 = 0$. These correspond to pairs of simple poles in the k_z-spectrum associated with modes guided by the infinite anisotropic screen. In free space, these modes radiate power at $z = \pm\infty$ and contribute to the active radiated power [imaginary part of the right-hand side of Eq. (30)] by half the residue around the pole. In a system which is periodic in z, there cannot be any radiation in this direction. Accordingly, the $H^2 = 0$ singularities only contribute to the reactive power, as one can check by letting $H^2 \to 0$ and $p \to k_y$, which only gives a real contribution to the right-hand side of Eq. (30). The $H^2 = 0$ resonances are an artifact resulting from the idealized modeling of the Faraday screen. In practice, Faraday screens are finite, covering a limited surface in front of the antenna straps and therefore, the contributions of the $H^2 = 0$ poles should be regarded as artificial in that case. This is less clear in the case of a low density plasma as indeed, the slow wave efficiently shields the parallel electric field. However, to investigate this question, plasma models more sophisticated than those considered here should be used. In the case of the IFS, the $H^2 = 0$ singularities should be neglected as far as possible. This is in contrast to the $p = 0$ singularities which may represent radiation toward $x \to -\infty$ in the periodic case (or in all directions in free space). Fig. 5 shows how strongly the spurious $H^2 = 0$ resonances can affect the propagation constant along the antenna. The parameters are $R = a = 2$ m, $d = 0.004$ m, $s = v = 0.002$ m, $w_y = 0.5$ m and $w_z = 0.125$ m. This figure also shows that the self-consistent current distribution calculated by ICANT closely matches the corresponding 2D estimate of Eq. (29). This kind of modeling problem no longer exists if a more realistic screen model is used, as ICANT allows.

5.3. The strap antenna with a finite Faraday screen

We now deal with one of the most interesting features of the self-consistent code, that is the possibility to model any part of the antenna structure by unknown current elements. Fig. 6 illustrates the whole system. Every screen blade is treated exactly as the strap itself, except that it has no active element. Here and in the following sections the finite screen will be defined by its length $2w_{ys}$ and width $2w_{zs}$, and its transparency $(L - l)/L$, where l is the blade width and L the period of the screen. It is very easy to vary the blade size or the screen transparency.

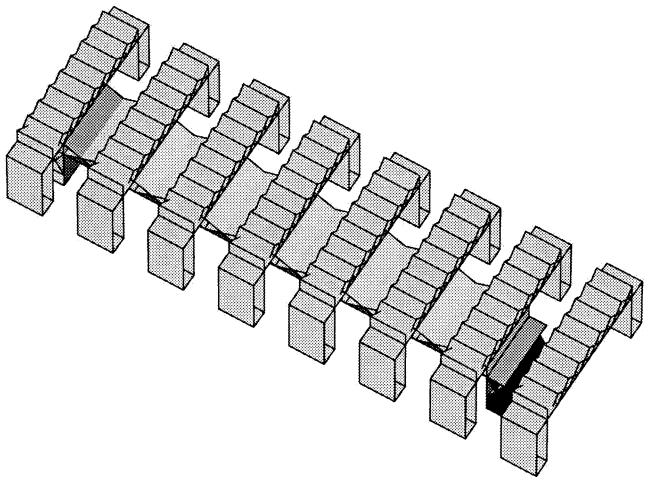

Fig. 6. Modeling of the strap antenna with its Faraday screen. The case shown is for unidirectional currents on both the strap and the screen.

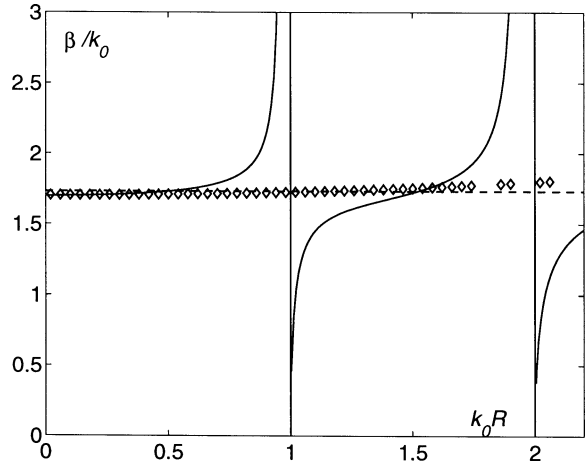

Fig. 7. The single strap antenna in vacuum with its finite Faraday screen. Variation of β/k_0 with the frequency. $R = a = 2$ m, $d = 0.004$ m, $s = 0.002$ m, $v = 0.004$ m, $w_y = 0.5$ m, $w_z = 0.125$ m, $w_{ys} = 0.75$ m, $w_{zs} = 0.5$ m. The screen transparency is zero (6 contiguous blades). The IFS resonances are shown by the solid lines. The dashed line corresponds to the static value, Eq. (28).

Of course, the number of current elements increases much due to the modeling of the screen. Fig. 7 displays the variation of the propagation constant with the frequency in the case of the FFS. The strap parameters are the same as on Fig. 5. The screen is made of six contiguous blades, with $w_{ys} = 0.75$ m and $w_{zs} = 0.5$ m. Here $s = 0.002$ m as previously and $v = 0.004$ m. The most striking result is the disappearing of the H^2 resonances plaguing the IFS model. For the low frequencies used in this example, the value of β obtained by the code agrees with the quasi-static prediction, Eq. (28). Due to self-consistency, the effective propagation constant β on the strap can then be varied simply by changing the screen transparency. This is shown on Fig. 8 where the screen transparency $(L - l)/L$ is varied from 0% (contiguous screen bars) to 100% (bar width zero), leading to a continuous decrease of β. For the case considered here (low frequency, $k_0 = 0.1$ m^{-1}) the values for the strap in vacuum or the strap shielded by an IFS agree with the transmission line theory. It is obvious that the realistic modeling of the screen results in a significant modification of the propagation constant which in turn has a definite influence on the radiated power.

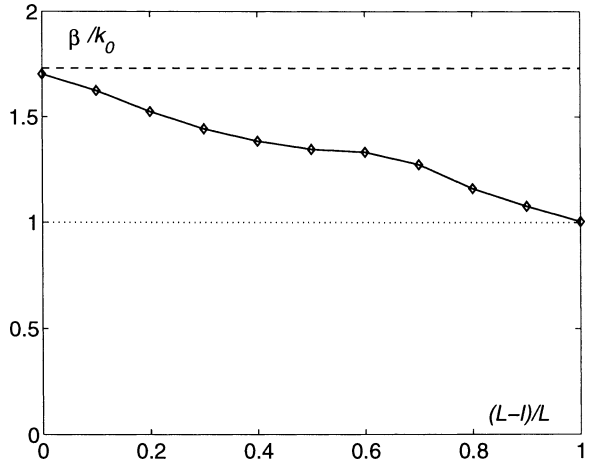

Fig. 8. The single strap antenna in vacuum with its finite Faraday screen. Variation of β/k_0 with the screen transparency. $k_0 = 0.1\ \mathrm{m}^{-1}$. Other parameters as on Fig. 7. The dashed line is the IFS limit, Eq. (28). The dotted line is the vacuum value $\beta/k_0 = 1$.

6. Magnetic shielding effects

In the previous models of straps and screen bars, the current was flowing on each ribbon only in one direction and with a flat distribution across the ribbon. In consequence, magnetic field lines were allowed to cross the conductors, contrary to what happens in real conductors, on which the normal component of the magnetic field has to vanish (§4). In this section, we shall remove these restrictions by allowing the current density to vary across conductors and to flow in any direction on their surface. This added freedom will allow the current distributions on the conductors to oppose the penetration of the normal component of the magnetic field, an effect we refer to as "magnetic shielding".

6.1. Transverse current profile of the single strap antenna

As a first example, let us consider a single strap antenna in vacuum (no Faraday shield), where we still impose a one-directional current, but we leave the transverse profile unknown. This is done by using A active elements on the feeder, with only the total current imposed (Fig. 9)

$$\sum_{j=1,A} f_j a_j = 1, \tag{32}$$

where the f_j's are weighting functions depending on the type of transverse current basis used. The theoretical expression for the current density on a strap isolated in free-space (total current 1 A) is

$$J_y(z) = \frac{1}{\pi} \frac{1}{\sqrt{w_z^2 - z^2}}. \tag{33}$$

For a strap close to the back-wall [limit of the plane capacitor, $(d-b)/w_z \ll 1$], due to the image currents in the back-wall, the current distribution is flat

$$J_y(z) = \frac{1}{2w_z}. \tag{34}$$

Fig. 10 shows the numerical result for a strap ($w_y = 0.5$ m, $w_z = 0.125$ m) located at a distance $d = 0.2$ m from the wall, and the comparison with the limiting distributions, (33) and (34). For the computation $R = a = 2$ m,

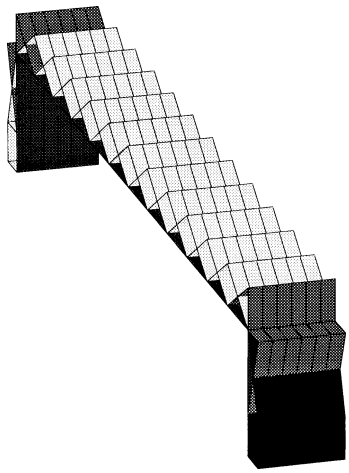

Fig. 9. Modeling of the antenna with a self-consistent transverse profile, for a unidirectional current. The active elements (in black) obey the Eq. (32).

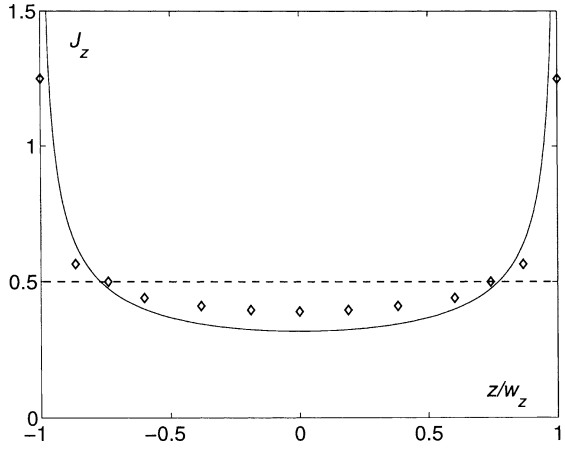

Fig. 10. Self-consistent transverse profile of the J_y current for the single strap (no Faraday shield) in vacuum. $R = a = 2$ m, $d = 0.2$ m, $v = 0.1$ m, $w_y = 0.5$ m and $w_z = 0.125$ m. $\diamond$: numerical results. Solid line: 2D theory, Eq. (33). Dashed line: capacitor limit, Eq. (34).

$v = 0.1$ m. The result of ICANT clearly lies in between the two limits, as it should. When the distance wall-strap decreases, the effect of the image currents increases and the self-consistent profile flattens. It has been checked that the transverse profile of the current has little influence on the radiated power. Hence most runs have been made with the simplest case of a flat transverse current profile on the strap.

6.2. Current loop formation

In order to correctly take magnetic shielding into account, the set of current elements should allow to represent current loops that oppose the penetration of the normal magnetic field in the conductors. Fig. 11 shows how the superposition of four roof-top current elements can represent such a current loop. It is to be noted that, although individually each current element carries a charge density, this choice of current elements allows having exactly $\nabla \cdot \mathbf{J} = 0$ if the solution requires it. This is not automatically the case for all choices of current elements. If this were not be the case, there would always exist a residual charge distribution varying on the mesh scale length, i.e.

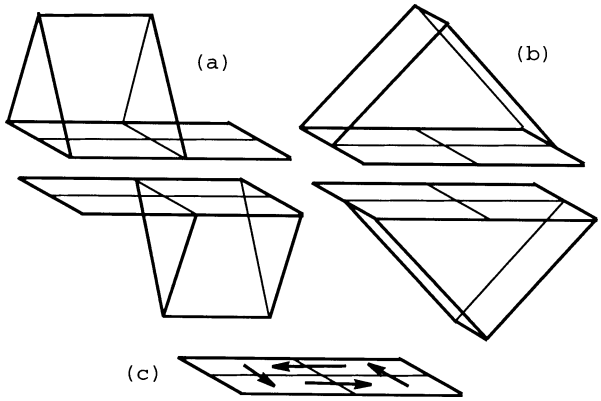

Fig. 11. Two rooftops (a) along one direction together with two rooftops, (b) along the perpendicular direction allow current loop formation, (c) with no residual charge.

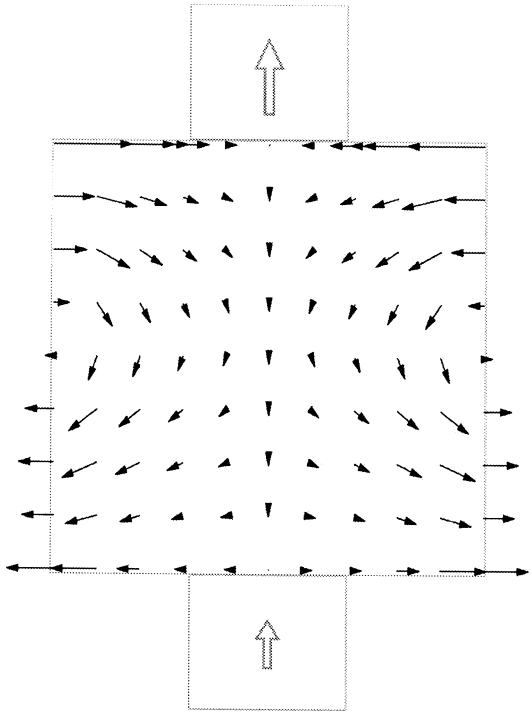

Fig. 12. Current loops induced by magnetic shielding effects on a screen plate. $R = 2$ m, $a = 2$ m, $d = 0.04$ m, $s = 0.05$ m, $v = 0.1$ m, $w_y = 0.5$ m, $w_z = 0.125$ m, $w_{ys} = w_{zs} = 0.25$ m, $k_0 = 0.2$ m^{-1}. The arrow length is proportional to the current amplitude. The currents at each end of the strap are shown at a reduced scale $(1/4)$ by the two large arrows.

with low convergence in Fourier spectrum, which could spoil the computation. In order to illustrate the magnetic shielding effect resulting from such a general current distribution, we consider a strap antenna covered by a large single FFS plate (in vacuum, with no IFS), on which we allow fully two-dimensional currents. The parameters are $R = a = 2$ m, $d = 0.04$ m, $s = 0.05$ m, $v = 0.1$ m, $w_y = 0.5$ m, $w_z = 0.125$ m, $w_{ys} = w_{zs} = 0.25$ m, and $k_0 = 0.2$ m^{-1}. Fig. 12 shows the formation of current loops that oppose to the magnetic field crossing the screen

plate. The current at the center of the wide screen bar runs opposite to that on the strap and the current loops close through the side parts of the bar (not shown) as the left- an right-most current arrows indicate. As the frequency is increased, the size of the current loops diminishes. If the screen bars are made narrower, as they are in more realistic cases, there is no longer current loop formation, but the image currents flowing on the screen have an influence on the radiated power. For not too low frequency and significantly wide screen blades, the magnetic shielding of the screen leads to a reduction in radiated power (by 20–30%) and to a lowering (by ≈10%) of the propagation constant β on the strap.

7. The magnetosonic wave in a homogeneous plasma

We now present results for the case of the simplest plasma model, a plasma with a density step, and the magnetosonic wave alone. We use this model to illustrate the features of the code because it is fast and allows to cover a wide range of parameters in a reasonable amount of time. It would be easy to input in the ICANT code the surface impedance matrix for the inhomogeneous plasma, obtained by any full-wave propagation code. Presently, two additional plasma models are available in the code: a step cold-plasma model including both the slow and the fast wave and an inhomogeneous plasma fast wave description (BRAFFA, §3). It is planned to include the inhomogeneous hot plasma wave code TOMCAT [22] in a near future.

7.1. Evolution of the radiated power with the plasma density

We consider a strap antenna with a finite Faraday screen and a homogeneous plasma. The parameters are as follows: $R = 4$ m, $a = 2$ m, $d = 0.05$ m, $s = 0.05$ m, $v = 0.1$ m, $w_y = 0.5$ m, $w_z = 0.125$ m, $w_{ys} = 0.7$ m, $w_{zs} = 0.375$ m, and the screen transparency is 50%. The magnetic field is $B_T = 3$ T and the plasma is deuterium. Fig. 13 shows the radiated power (for a unit peak current on the antenna) versus the plasma density and the frequency. The maximum power coupled to the plasma increases with the frequency. The optimal density for

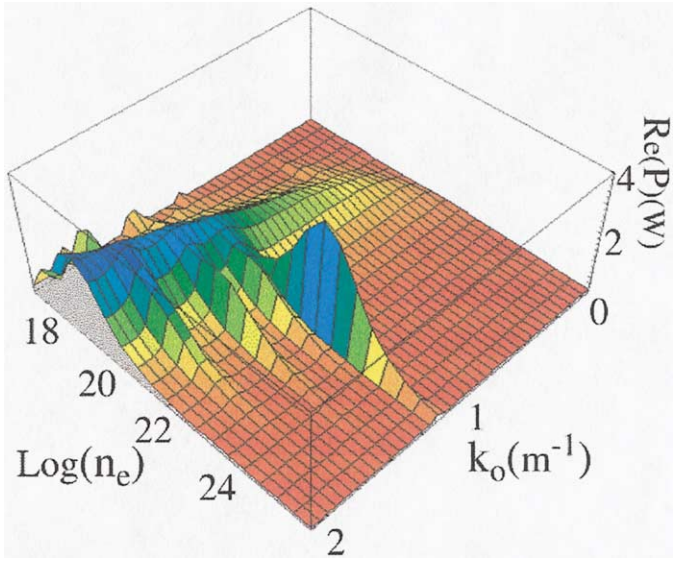

Fig. 13. The power radiated by an antenna coupling to the fast magnetosonic wave, versus the electron density and the frequency. The parameters are $R = 4$ m, $a = 2$ m, $d = 0.05$ m, $s = 0.05$ m, $v = 0.1$ m, $w_y = 0.5$ m, $w_z = 0.125$ m, $w_{ys} = 0.7$ m, $w_{zs} = 0.375$ m. The screen transparency is 50%.

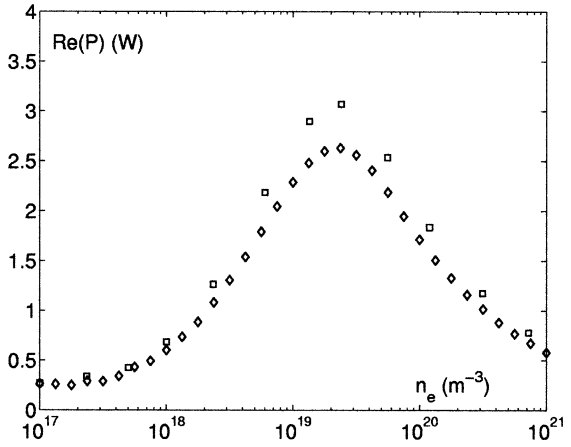

Fig. 14. The power radiated by a strap antenna (no Faraday shield) coupling to the fast magnetosonic wave for a plasma step. Comparison of the ICANT results (◇) with the BRACC results (□). The parameters are $R = a = 2$ m, $d = 0.06$ m, $v = 0.03$ m, $w_y = 0.5$ m, $w_z = 0.125$ m, $B_T = 6$ T, $k_0 = 0.6$ m^{-1}.

maximum coupling slightly decreases with frequency. Screen-guided modes appear at low density, as expected from the discussion in §3.1: since the low density limit of the surface impedance matrix of the magnetosonic wave is the IPS, characteristics of the IFS modeling are found. Co-axial modes excited by the J_x currents appear at very high densities because at these densities, the plasma behaves almost like a perfect conductor. Co-axial modes have been discussed in [14] (and references therein). Depending on the specific case, they can be considered as part of the real physical situation or not. The ICANT code provides ways of neglecting or replacing these $p^2 = 0$ resonant contributions if required [20]. Finally, Fig. 14 shows the good agreement of ICANT with the predictions of the code BRACC [15], used in the step plasma limit. The comparison is made for a single strap (no Faraday shield), with $R = a = 2$ m, $d = 0.06$ m, $v = 0.03$ m, $w_y = 0.5$ m, $w_z = 0.125$ m, $B_T = 6$ T and $k_0 = 0.6$ m^{-1}. As the currents are not self-consistently computed in BRACC, this code used the β values computed by ICANT as input parameters. The behaviour of the coupled power versus frequency and density remains globally similar for the case of inhomogeneous plasma. Quantitative differences can, however be important. In particular, for a given frequency, the maximum radiated power is reached only for values of the central density much larger than in the plasma-step case. For practical simulations, the inhomogeneous plasma model is used.

7.2. The tunable strap antenna

Some antennas, like those of Tore-Supra [26] or those planned for ITER-FEAT [23] are installed with pre-matching elements (usually capacitors) that make them resonant. Although the modeling of the whole system including those matching elements that are behind the wall is a very complicated task, it is interesting as a first step to include in the model end capacitors. This allows computation of the self-consistent current distribution and the frequency response of the antenna with these pre-matching elements. The tunable capacitors are modeled by additional straps, whose distance to the wall can be changed to achieve the resonance condition. This method can be used only if the distance between the wall and these additional straps stays small compared to the distance of the main strap. Several different models of capacitors can be used, Fig. 15 shows one example. For $R = 2.35$ m, $a = 0.74$ m, $d = 0.09$ m, $v = 0.18$ m, $w_y = 0.5$ m, $w_z = 0.05$ m, Fig. 16 shows the evolution of the radiated power with frequency, for three different distances of the additional strap to the back-wall ($d - b_1 = 0.005$ m, 0.01 m and 0.05 m), in order to simulate three different choices of the value of the tuning capacitance. The plasma has a density of $3 \cdot 10^{19}$ m^{-3} and the magnetic field is 3 T. The system is clearly resonant at a particular frequency, which depends upon the tuned strap-wall distance. We emphasize that this resonance is a true antenna resonance, resulting

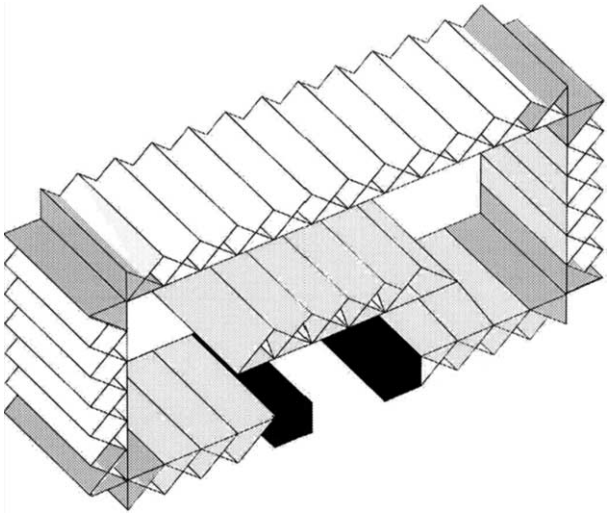

Fig. 15. Modeling of a tunable strap antenna. There are two active elements (black) and the tuning is obtained by varying the distance of the capacitor strap to the wall.

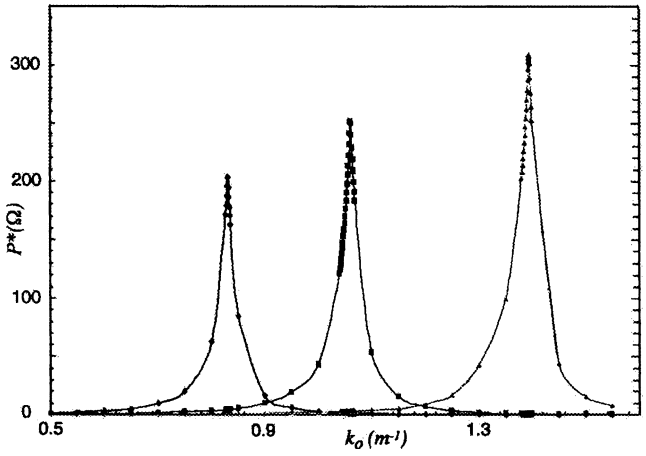

Fig. 16. The radiated power for the tunable strap (no Faraday screen), versus the frequency. The strap parameters are those of the Tore-Supra antenna, $R = 2.35$ m, $a = 0.74$ m, $d = 0.09$ m, $v = 0.18$ m, $w_y = 0.5$ m, $w_z = 0.05$ m. Plasma step model, $n_e = 3 \cdot 10^9$ m^{-3}, $B_T = 3$ T. Three different values of the distance of the tuning strap to the wall are shown ($d - b_1 = 0.005$, 0.01 and 0.05 m, from left to right), leading to three different resonant frequency values.

from the electrical matching of the antenna-plasma system, in contrast with the $p^2 = 0$ or $H^2 = 0$ transverse mode resonances encountered previously.

7.3. Modeling antennas with thick conductors

In all the above examples, all the antenna parts have been modeled by infinitely thin conductors. As a thick conductor is nothing but a volume enclosed in an infinitely thin conducting surface, by combining thin conducting elements, ICANT also allows to represent currents flowing on thick conductors. As an example Fig. 17 shows a strap antenna with 7 thick screen bars. The parameters are $R = 2.35$ m, $a = 0.74$ m, $d = 0.06$ m, $v = 0.18$ m,

$w_y = 0.5$ m, $w_z = 0.05$ m, $w_{ys} = 0.65$ m and $w_{zs} = 0.25$ m. The screen front (facing the plasma) is at $s = 0.12$ m. The screen transparency is 50% (each bar is 0.1 m wide). The wave frequency is 48 MHz. The plasma is modeled by a density step, $n_e = 5 \cdot 10^{19}$ m^{-3}, the magnetic field $B_0 = 3$ T. The case shown on Fig. 17 is for a thickness of 0.04 m. The arrows on different parts of the screen represent the average (vector) current on these parts. The current on the strap itself is represented by arrows at a reduced scale (1/4). ICANT has been run for 5 values of the bar thickness: 0.005, 0.02, 0.04, 0.06 and 0.08 m (the distance between the back of the screen and the strap decreases accordingly). Fig. 18 shows that the radiated power (for a given peak current on the ground element) increases linearly with the thickness. Fig. 17 shows that the y-component of the current on the screen front flows in the same direction than the current on the strap and is closer to the plasma, hence it efficiently contributes to the power. One can note, however, that magnetic shielding effects at first cause a decrease of the radiated power compared to the infinitely thin screen case (asterisk on Fig. 18). This adverse effect was already discussed by Faulconer [24]. Similarly the propagation constant β on the strap starts from a lower value than for the thin screen value (1.09 instead of 1.096) and increases slightly with the bar thickness (Fig. 19). The antenna spectrum is also

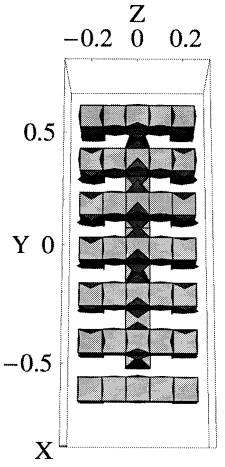

Fig. 17.

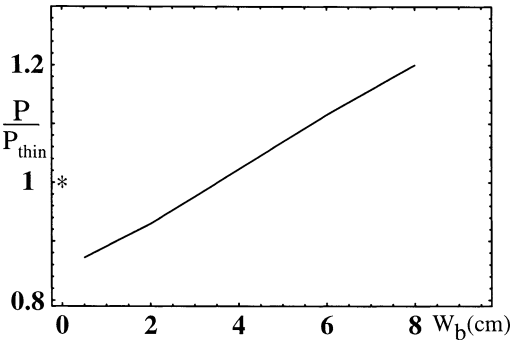

Fig. 18.

Fig. 17. A single strap antenna and its thick blade screen. The triangles indicate the intensity of the current components on every side of the screen blades. The arrows for the current on the strap are drawn at a reduced scale (1/4).

Fig. 18. Variation of the radiated power (for a peak current of 1 A on the strap) with the thickness w_b of the screen bars, for the antenna of Fig. 17. The asterisk represents the value for the thin screen case.

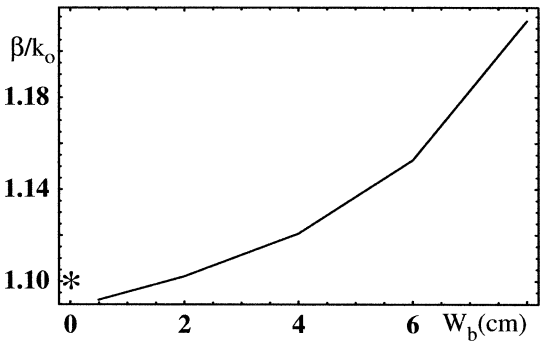

Fig. 19. Variation of the propagation constant β on the strap with the thickness w_b of the screen bars, for the antenna of Fig. 17. The asterisk represents the value for the thin screen case.

modified [25], although it is difficult to infer the effect on the coupling. Of course, the modeling of thick conductors significantly increases the number of elements in the computation.

7.4. Fields between the screen and the plasma

Another important feature of the ICANT code is that, due to the realistic modeling of the screen, it can compute the fields in the whole region between the screen and the plasma. This is particularly important if the screen or antenna geometry is such as to cause large electric field concentrations. For such a detailed modeling, it is important to incorporate all the required geometrical features of the screen, and, in particular, the fact that many shielded antennas have slanted Faraday shields. This feature is also available in ICANT as illustrated by the Tore-Supra antenna model described in [26]. Fig. 20 shows contour plots of the longitudinal component of the electric field E_z. Here we model a two-strap structure shielded by a six blade screen and surrounded by bumpers, similar to the Tore-Supra antenna. The parameters are $d = 0.09$ m, $s = 0.02$ m, $v = 0.04$ m, $w_y = 0.5$ m, $w_z = 0.05$ m, $w_{ys} = 0.65$ m and $w_{zs} = 0.25$ m. The distance between the straps is 0.26 m. The screen transparency is 50% and the wave frequency is 48 MHz. At $x = -v$ the plasma density is 10^{18} cm^{-3}; it reaches $n_e = 5 \cdot 10^{19}$ cm^{-3} at the center with a parabolic density profile. The magnetic field is $B_0 = 3$ T. There are 697 current elements and the field is calculated in a plane at 0.5 cm in front of the screen. The antenna operates in a dipole mode, with a $(0, \pi)$ phasing. The radiated power is 1 MW. It is clear that the E_z component is excited by the J_x current flowing on the parts connecting the screen blades to the wall, and on the bumpers. The detailed knowledge of the electromagnetic field around the antenna, and in particular the electric field component parallel to the total static magnetic, is very important if sheath effects are suspected to lead to hot spots or other adverse consequences like impurity generation (see, e.g., [27]). Indeed, the computation of RF sheaths necessarily rests on the detailed evaluation of electromotive forces induced along field lines in the vicinity of the antenna [28].

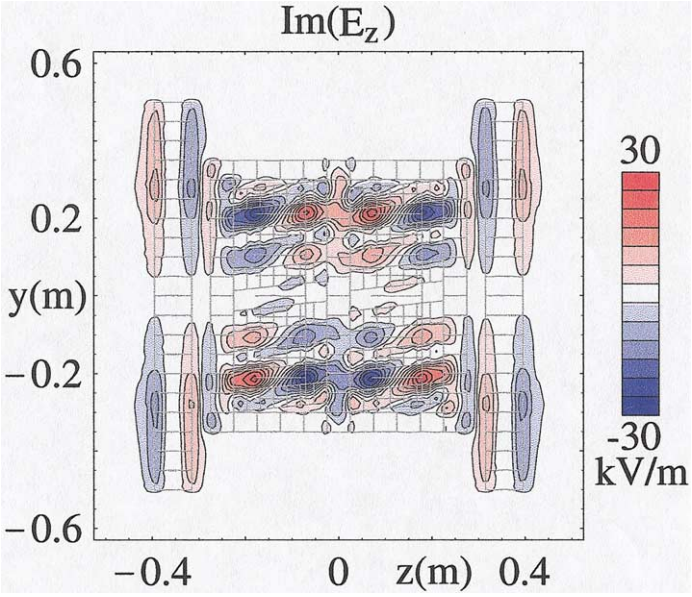

Fig. 20. Contour lines of the z-component of the electric field at the distance of 0.5 cm from the screen, for a two-strap structure similar to the Tore-Supra antenna.

8. Conclusion

The present code ICANT has been developed mainly in view of application to antenna systems for the ion cyclotron heating of strongly magnetized fusion plasma. However, because of the independence of the formalism on the particular choice of plasma wave description, the code could as well be useful in many other situations where the geometry is similar, e.g., antennas mounted on rockets traveling in the ionosphere or antennas radiating into (or generating) process plasmas enclosed into rectangular-shaped boxes. Incidentally, there is no major difficulty in transforming the periodic boundary condition in the transverse directions (y, z) to the metallic boundary conditions relevant to a conducting rectangular box (see [21], where this is done for the 2D case). Only the basic geometry of an antenna radiating in front of a back wall into a transversely homogeneous plasma is to be respected.

In the present implementation, most current elements remain tightly linked to the Cartesian geometry, i.e. were chosen to lie in co-ordinate planes. Rotation in the (y, z) plane is trivial but any other rotation is not, because of the distinct treatment of the x-direction. The development of further oblique elements is under investigation. The present current elements all have rectangular support. It would also be possible to implement current elements with triangular support, at the expense of increased complexity of the algebra, larger number of elements and more involved book-keeping.

We have shown that the present version of the ICANT code can compute self-consistently the solution of the ICRH problem in most cases of practical relevance. The modeling of the antenna by finite current elements and the formulation of the problem as a consistency condition for the current allow to determine the currents on the strap, on the blades of its Faraday screen and generally speaking on any piece of conductor lying around the antenna. Standard quantities like the equivalent propagation constant, the radiated power and the electric field in the whole vacuum region are provided. It was shown that the classical results are recovered in a variety of classical configurations and the results with plasma have been cross-checked with the earlier non self-consistent code BRACC. Although the present version allows only considering single-wave inhomogeneous or cold two-waves homogeneous plasma, the method could easily account for the propagation of several waves in an inhomogeneous plasma, and an upgrade is planned. The code can be used without difficulty for more complex situations, for example, arrays of antennas, where several straps are shielded by a single screen with many blades, and surrounding elements protecting the antenna (septa and bumpers). Of course the computation time increases quickly with the number of current elements that are chosen, but realistic antenna structures could be handled in a reasonable amount of time on an efficient workstation.

References

[1] G. Cattanei, R. Croci, Nucl. Fusion 17 (1977) 239.
[2] J. Adam, Report EUR-CEA-FC 1004, 1979.
[3] V.P. Bhatnagar, R. Koch, A.M. Messiaen, R.R. Weynants, Nucl. Fusion 22 (1982) 280.
[4] K. Theilhaber, J. Jacquinot, Nucl. Fusion 24 (1984) 541.
[5] S. Puri, Phys. Fluids 27 (1984) 2156.
[6] M. Saigusa, T. Yamamoto, C.C. Petty, K. Yoshnoka, H. Kazumi, H. Kawashima, T. Fuju, H. Kimura, Y. Miura, H. Tamai, Nucl. Fusion 33 (1993) 421.
[7] M.D. Carter, D.A. Rasmussen, P.M. Ryan, G.R. Hanson, D.O. Stellings, D.B. Batchelor, T.S. Bigelow, A.C. England, D.S. Hoffman, M. Murakami, C.Y. Wang, J.B. Wilger, J.R. Rogers, J.R. Wilson, R. Majeski, G. Schilliony, Nucl. Fusion 36 (1996) 209.
[8] Y.L. Ho, W. Grossmann, A. Dobrot, M.D. Carter, P.M. Ryan, D.B. Batchelor, 10th Top Conf. RF Power in Plasmas, Boston, AIP Conf. Proc. 289 (1993) 359.
[9] J.R. Myra, D.A. D'Ippolito, Y.L. Ho, Three-dimensional analysis of antenna sheaths, Fusion Engrg. Design 31 (1996) 291–312.
[10] G. Vecchi, M. Riccitelli, R. Maggiora, Nucl. Fusion 39 (1999) 1403.
[11] M. Söll, F.J. Fischer, J.-M. Noterdaeme, H. Welder, in: 18th MSC Conf., Prien, 1991.
[12] R. Koch, P.U. Lamalle, D. Van Eester, Plasma Phys. Control. Fusion 40 (1998) A191.
[13] M. Porkolab, A. Bécoulet, P.T. Bonoli, C. Gormezano, R. Koch, R.J. Majeski, A.M. Messiaen, J.-M. Noterdaeme, C. Petty, R. Pinsker, D. Start, R. Wilson, Plasma Phys. Control. Fusion 40 (1998) A35.

[14] R. Koch, V.P. Bhatnagar, A.M. Messiaen, D. Van Eester, Comp. Phys. Comm. 40 (1986) 1.
[15] P. Decamps, R. Koch, R. van Nieuwenhowe, G. van Oost, G. van Wassenhove, T. Delvigne, A.M. Messian, P.E. Vandenplas, R.R. Weynants, Plasma Phys. Control. Fusion 33 (1991) 1109.
[16] A.K. Ram, A. Bers, Nucl. Fusion 24 (1984) 679.
[17] M. Brambilla, Nucl. Fusion 35 (1995) 1265.
[18] I.P. Pavlov, J.A. Heikkinen, Effect on the antenna orientation and plasma anisotropy on the directivity of fast wave antenna radiation, Phys. Plasma 2 (1995) 3573.
[19] A.M. Messiaen, R. Koch, V.P. Bhatnagar, M.P. Evrard, M. Luwel, P.E. Vandenplas, R.R. Weynants, Theoretical aspects of the coupling properties of ICRH antennae, in: Proc. 3rd joint Varenna—Grenoble Int. Symposium on Heating in Toroidal Plasmas, 1982, p. 243.
[20] S. Pécoul, PhD Thesis, Nancy, France, 1998.
[21] R. Koch, LPP-ERM/KMS Brussels Report n° 106, 1996.
[22] D. Van Eester, R. Koch, Plasma Phys. Control. Fusion 40 (1998) 1949–1975.
[23] G. Bosia, K. Ioki, N. Kobayashi, P. Bibet, R. Koch et al., Design of ITER-FEAT RF Heating and Current Drive Systems, in: 18th IAEA Fusion Energy Conf., Sorrento, 2000, paper IAEA-CN-77/ITERP/14.
[24] D.W. Faulconer, J. Appl. Phys. 54 (1983) 3810–3817.
[25] S. Pécoul, S. Heuraux, R. Koch, G. Leclert, A. Bécoulet, L. Colas, ICANT code: a tool to compute the characteristics of ICRH antennae with realistic structures and their near fields, 27th EPS Conference on Controlled Fusion and Plasma Physics, Budapest, Europhys. Conf. Abstracts 24B (2000) 388–391.
[26] S. Pécoul, S. Heuraux, R. Koch, G. Leclert, A. Bécoulet, L. Colas, Self-consistent computations of the electric field near ICRH antennas. Application to the Tore Supra antenna, 13th Topical Conf. on Applications of Radio Frequency Power to Plasmas, Annapolis, AIP Conf. Proc. 485 (1999) 361–364.
[27] L. Colas, L. Ladurelle, G. Agarici, V. Basiuk, B. Beaumont et al., Thermal behaviour of ICRH antennas on Tore Supra, 13th Topical Conf. on Applications of Radio Frequency Power to Plasmas, Annapolis, AIP Conf. Proc. 485 (1999) 128–131.
[28] L. Colas, M. Bécoulet, L. Costanzo, S. Pécoul, S. Heuraux et al., Heat Load Patterns on Tore Supra ICRH Antennas, 27th EPS Conf. on Controlled Fusion and Plasma Physics, Budapest, Europhys. Conf. Abstracts 24B (2000) 792–795.